Power Management of a Self-Powered Multi-Parameter Wireless Sensor for IoT Application

Dingyi He, *Student Member*, *IEEE* and Babak Fahimi, *Fellow*, *IEEE*
Renewable Energy and Vehicular Technology Laboratory
The University of Texas at Dallas
Dingyi.he@utdallas.edu

***Abstract*—This paper proposes a power management system for a self-powered wireless sensor that is designed for health monitoring of electric machines through analysis of the recorded vibration and temperature. Implementation of Internet of Things permits use of the monitoring methods based on machine learning and artificial-intelligence (AI). In order to accommodate a versatile and feasible implementation of such monitoring system, a self-powered multi-sensor wireless platform is desired. The proposed power management is based on an analog realization, which has low power consumption and by the virtue of the device multiplexing (i.e. energy harvesting and sensing) technology reduces the cost. A simple and effective control method is introduced and experimental results illustrating a monitoring time of the sensor of 19 seconds is captured.**

Keywords— Energy Harvesting, Motor Condition Monitoring, Motor Fault Diagnose, Multi-source, Wireless Sensor, Power Management

I. INTRODUCTION

Electrification of conventional mechanical systems and the use of adjustable speed motor drives in domestic and industrial applications is on the rise. This transformation is driven by the quest for higher efficiency, more reliable and interactive operation, and saving the environment. [1]. Safety is one of the main concerns in electrified systems. The conditions of electric machines in an electrified system such as electric vehicles (EV), EV-bus, and electrified tram are critical from a safety viewpoint. In order to prevent severe accidents caused by motor fault, online motor condition monitoring and fault diagnosis are necessary. Methods for motor monitoring and fault diagnosis are developed extensively in the literature since the inception of electric machinery [2]. These methods can be categorized as

1) current spectrum analysis,
2) vibration analysis,
3) temperature analysis,
4) radio-frequency (RF) emissions analysis, and
5) electromagnetic (EM) field monitoring [2-4].

However, these methods usually have the following drawbacks:

1) imprecise fault discrimination because same signature can be caused by different faults,
2) limited applicability to variable speed motor,
3) limited applicability to online estimation [3].

In order to solve these problems, many efforts have been spent to apply machine learning and artificial-intelligence (AI) technologies to motor fault prediction and condition monitoring [2, 3]. However, these methods require strong computational platforms and large storage capability that normal on-board microcontroller units (MCUs) cannot provide. Hence, the concept and technologies of Internet of Thing (IoT) have attracted much attention to improve AI-based motor health monitoring system [5]. In these motor condition monitoring methods, only the current spectrum data can be directly measured by the motor drive system, and the remaining methods require additional sensors. Recently, new methods incorporating temperature and vibration of the stator have been reported. These methods use a multi-signal sensing system IoT [5], and additionally self-powered multi-signal wireless sensors are desired.

There are several self-powered wireless sensors for motor condition monitoring that are published recently [6, 7]. However, most of them use different devices for energy harvesting and data collection. For these monitoring methods, the data sources (vibration, temperature, RF emission, and EM field) can also produce power ranging from micro-watts (μW) to mili-watts (mW) through transducers [8], such as piezoelectric transducer, thermoelectric generator (TEG), and RF antenna. Meanwhile, piezo plays the role of vibration detector and RF antenna can be used for communication or RF emission detection. There are few papers that report self-powered wireless sensors based on energy harvester/transducer multiplexing technology [9].

Most of these sensors are single-parameter and single energy source, which is a shortage because that single energy source sensor depends highly on the environment. It will consequently cause short operation time resulting in insufficient collection of data for analysis.

Hence, multi-source energy harvesting is desired for motor health monitoring sensor platform. There are some publications introducing multi-source energy harvesting [10-15]. Some of them use MCU, which introduce high-power consumption, to decrease the system scale [15, 16].

The proposed power management system in this paper is targeted towards a self-powered multi-signal sensing system

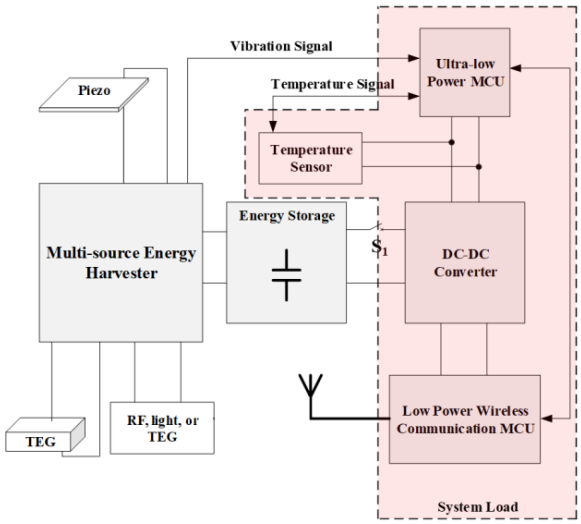

Fig. 1. Sensor system architecture

used for motor health monitoring. This system does not contain a microprocessor so that the power consumption of the control is lower than microcontroller embedded system. Additionally, the energy harvesting sub-system is a multi-source harvester depending on availability of the sources.

II. System Architecture

Fig.1 shows the system architecture. The proposed system has three energy sources. The AC source is the piezoelectric transducer. This piezo-electric device provides energy and vibration signal to the system. The DC source represents a thermoelectric generator (TEG). During the operation of the motor in the system, there is temperature difference between motor surface and environment. Hence, TEG provides constant and stable energy to the sensor.

In an electrified environment, RF energy can be obtained from on-board Wi-Fi, external communications and sensor network communications, and light may exist as well. Therefore, depending on the environment, the third energy source (axillary source) can be RF antenna and its rectifier, photovoltaics film, or TEG.

These energy sources are connected to a multi-source energy harvesting circuit whose control system does not contain any micro-controller. This energy harvester is analyzed in detail in the next section. This circuit charges the energy storage unit (ESU), which consists of a storage capacitor ($C_{storage}$). A switch S_1 connects the ESU and the system load.

The system load consists of a DC-DC converter, a digital temperature sensor, an ultra-low power MCU (TI MSP432), and a low power wireless communication MCU (TI CC2650). The DC-DC converter regulates the voltage (V_{DC}) to support the sensing and communication sub-system of the sensing system. MSP432 is the main MCU of the sensing and communication sub-system. It records the vibration signal and the data from temperature sensor and sends data to CC2650 for wireless communication. The main MCU also manages the sleep/weak actions of the digital subsystem.

The system has three operation modes: load-on mode, load-sleep mode, and load-off mode. The operation mode control is hysteresis control. The energy harvester continuously charges the ESU when energy sources are available. Once the voltage of ESU reaches the load-on hysteresis boundary during the fresh charge process (shown in Fig. 3), S_1 turns on and the system load starts consuming power. Once the voltage of ESU falls back to load-sleep boundary, the MCUs enter sleep mode to reduce energy consumption. If the voltage of the ESU further decreases to load-off boundary, S_1 turns off and loads shut down.

Fig. 2 illustrates an example of the system operation through a time vs. $C_{storage}$ voltage ($V_{Cstorage}$) curve. At the beginning, $C_{storage}$ is fully discharged. The system is at fresh charge period. Since the output power of the energy harvester circuit is environment-dependent, the charging speed is not steady. At $t = t_0$, $V_{Cstorage}$ reaches the load-on threshold. At this point, S_1 turns on by analog control circuit. $C_{storage}$ provides energy to the system load. Since the power consumption of the load is higher than the charging power, $V_{Cstorage}$ decreases. At instant t_1, $V_{Cstorage}$ decreases to load-sleep boundary, and the MCUs enter sleep mode. Therefore, the power consumption of the load is lower than the charging power, and $V_{Cstorage}$ starts increasing. At $t = t_2$,

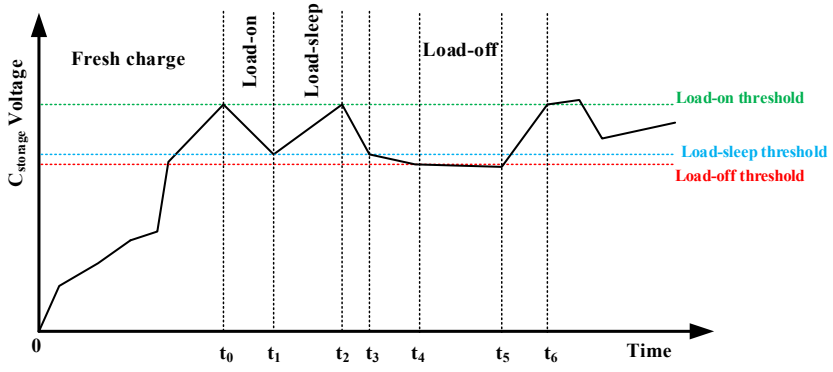

Fig. 2. Time vs. storage capacitor voltage – example of system operation

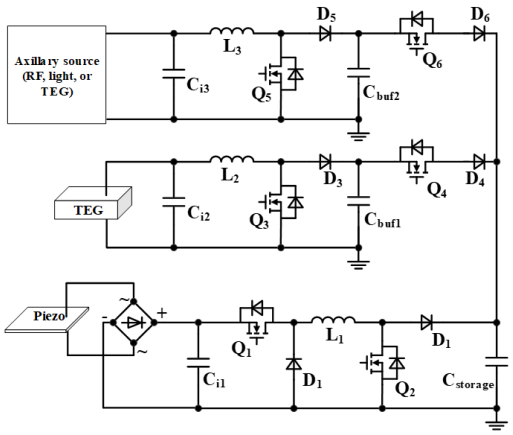

Fig. 3. Power stage of the energy harvester

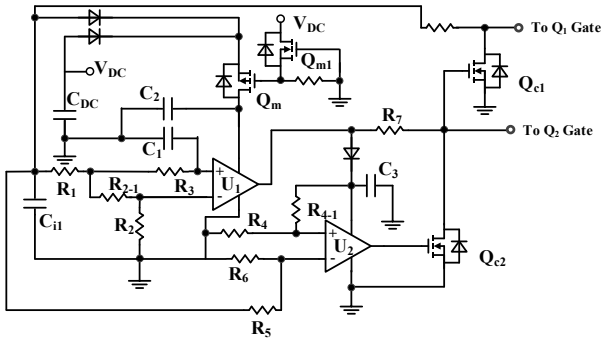

Fig. 4. Peak and zero detector

system enters load-on mode by the command of main MCU. At $t = t_3$, even in load-sleep mode, the power consumption of the load is higher than the charging power, so that $V_{Cstorage}$ keeps decreasing. Finally at $t = t_4$, $V_{Cstorage}$ decreases to load-off boundary, and S_1 turns off.

III. Multi-Source Energy Harvester

Many multi-source energy harvesters have been investigated over the past decade. Some of the publications concentrate on reducing the scales of the circuit, which requires less number of inductors. Consequently, in these circuits, the control loop is complicated so that the use of a MCU becomes mandatory.

A. Power Stage

As shown in Fig. 3, there are three energy sources: piezo, TEG, and axillary source. Piezo is the AC source that charges C_{i1} through a diode rectifier. C_{i1} is the input capacitor. Once the voltage of C_{i1} (V_{Ci1}) reaches the peak value, MOSFETs Q_1 and Q_2 turn on, and C_{i1} resonates with L_1. V_{Ci1} decreases and energy flows from C_{i1} to L_1. When V_{Ci1} decreases to a certain value (e.g. the threshold gate voltage of Q_1), Q_1 and Q_2 turn off so that L_1 will resonate with $C_{storage}$ and C_{i1} starts charging again. Energy flows from L_1 to $C_{storage}$.

The DC source is TEG and the axillary source can be RF antenna and its rectifier, photovoltaics film, or TEG. They charge the buffer capacitor C_{buf1} and C_{buf2} through boost DC-DC converters, respectively. The control of the valve MOSFETs (Q_4 and Q_6) is based on hysteresis control. Once the voltage of any of the buffer capacitors (V_{Cbuf1} or V_{Cbuf2}) increases to the upper boundary, corresponding switch turns on and energy flows from the buffer to $C_{storage}$. Then, V_{Cbuf1} or V_{Cbuf2} decrease to lower boundary and as such the corresponding switch turns off.

Notice that, since resonance happens between L_1 and $C_{storage}$, the piezo charge will always be the primary even if Q_4 and Q_6 turn on. Therefore, the energy stored in C_{i1} immediately transfers to $C_{storage}$ when V_{ci1} reaches the peak and energy waste is prevented.

B. Control Circuit

In order to save power consumption of the control circuit, there are only analog devices in use.

For the AC source part, a peak-zero detector (Fig. 4) is required. As shown in Fig. 4, U_1 and U_2 are nano-power comparators. C_{i1} is the same capacitor shown in Fig.3, which is the input capacitor of piezo part. C_{DC} is the output capacitor of the DC-DC converter in Fig. 1. The marked Q_1 Gate and Q_2 gate are the gates of the same MOSFETs marked in Fig. 2.

U_1 is used for the peak detection and C_2 provides energy to it. Notably the voltage of C_2 depends on maximum value of V_{Ci1} when system is in load-off mode, and it equals V_{DC} (the output voltage of the DC-DC converter) in load-sleep mode. Q_m and Q_{m1} form an enabler to turn on and off the AC energy harvesting part. Q_{m1} turn on during load-on mode so that the vibration measurement is not influenced by the energy harvester. R_1, R_2 and $R_{2\text{-}1}$ are the voltage divider for V_{Ci1}. R_3 and C_1 form a RC delay circuit so that the positive input of U_1 follows its negative input with a short delay. Hence, during raising slope of V_{Ci1}, U_1 outputs 0 volt. When V_{Ci1} reaches the peak, the negative input of U_1 starts to decrease and positive input becomes larger. Consequently, U_1 outputs high level voltage so that Q_{c1}, Q_1, and Q_2 turn on and C_3 is charged. C_{i1} resonates with L_1.

Then, U_2 starts work to detect the zero-point (the turn-off point of Q_1 and Q_2) and C_3 provides energy to U_2. Since the voltage of C_3 remains at the peak value of V_{Ci1}, the resistors $R_{4\text{-}1}$, R_4, R_5, and R_6 form two voltage dividers that determine the zero-point voltage of C_{i1}. At this point, Q_{c2} turns on and Q_{c1}, Q_1, and Q_2 turn off. In load-sleep mode the zero-point voltage is V_{zp} shown in equation (1).

$$V_{zp} = \frac{R_4\left(R_5 + R_6\right)}{R_6\left(R_{4-1} + R_4\right)} V_{DC} \tag{1}$$

where V_{DC} is the output voltage of the DC-DC converter, R_3, R_4, R_5, and R_6 are shown in Fig. 4

Fig. 5 shows the control circuits that control Q_4 and Q_6 in Fig. 2. R_{h1}, R_{h2}, R_{h3}, and Q_{h1} form the hysteresis voltage divider for the gate of Q_{h2}. C_{bufx} is the buffer capacitor C_{buf1} or C_{buf2} in Fig. 2. The hysteresis boundary is shown in (2) and (3).

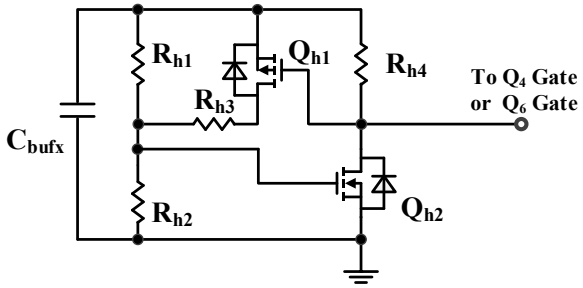

Fig. 5. Hysteresis gate controller

$$V_{HT} = \frac{R_{h1} + R_{h2}}{R_{h2}} V_{GT} \tag{2}$$

$$V_{LT} = \frac{R_{h1}R_{h2} + R_{h1}R_{h3} + R_{h2}R_{h3}}{R_{h2}\left(R_{h1} + R_{h3}\right)} V_{GT} \tag{3}$$

where V_{HT} is the upper hysteresis boundary, V_{LT} is the lower hysteresis boundary, V_{GT} is the gate threshold voltage of Q_{h2}, and R_{h1}, R_{h2}, and R_{h3} are as shown in Fig. 5.

The quiescent power consumption of control circuits shown in Fig.4 and Fig. 5 is described in (4).

$$P_{loss} = U_{in}(I_{qc} + 2I_{inc} + I_{ql}) + \frac{{U_{in}}^2}{R_1 + R_2} + \frac{{U_{in}}^2}{R_5 + R_6} + 2\left(\frac{{U_{buf}}^2}{R_{h1} + R_{h2}} + U_{buf} I_{ql1}\right) \tag{4}$$

where P_{loss} is the quiescent control power consumption, U_{in} is the input voltage of piezo part, I_{qc} is the quiescent current of the comparator, I_{inc} is the input current of the comparator terminal, I_{ql} is the leakage current of Q_{c1} shown in Fig. 4, U_{buf} is the buffer capacitor voltage, I_{ql1} is the leakage current of Q_{h2} shown in Fig. 5, and the resistors are shown in Fig. 4, and Fig. 5, respectively.

The maximum power consumption of control circuits shown in Fig. 4 and Fig. 5 is described in (5).

$$P_{mloss} = U_{in}(4I_{inc} + I_{ql} + I_{gl2}) + \frac{{U_{in}}^2}{R_1 + R_2} + \frac{{U_{in}}^2}{R_7} + \frac{{U_{in}}^2}{R_3 + R_4} + \frac{{U_{in}}^2}{R_5 + R_6} + 2\left(\frac{(R_{h1} + R_{h2}){U_{buf}}^2}{R_{h1}R_{h2} + R_{h2}R_{h3} + R_{h1}R_{h3}} + U_{buf} I_{ql1} + \frac{{U_{buf}}^2}{R_{h4}}\right) \tag{5}$$

where P_{aloss} is the maximum control power consumption, I_{gl2} is the leakage gate current of Q_{c2} shown in Fig. 4, and the resistors are shown in Fig. 4, and Fig. 5, respectively.

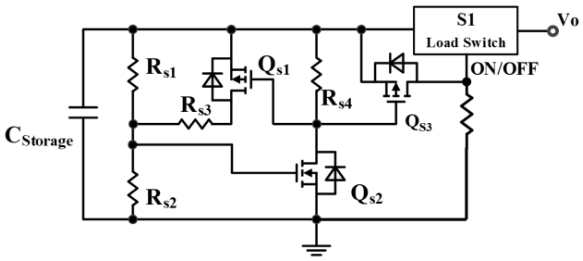

Fig. 6. Control circuit for load switch

IV. Sensing Sub-System

As described above, the sensing and digital sub-system is seen as a load to the proposed power management circuit. S_1 shown in Fig. 1 controls the operation mode (load-on and load off). The load-off/load-on mode switching (e.g. t_0, t_4 and t_6 moments in Fig. 3) are controlled by the hysteresis voltage divider circuit shown in Fig. 6. The storage capacitor $C_{Storage}$ is the same one shown in Fig. 3 and the load switch $S1$ is the same load switch as in Fig. 1. (i.e. Similar to hysteresis gate controller shown in Fig. 5). The hysteresis boundary is described in (6) and (7).

$$V_{HS} = \frac{R_{S1} + R_{S2}}{R_{S2}} V_{GQ2} \tag{6}$$

$$V_{LS} = \frac{R_{S1}R_{S2} + R_{S1}R_{S3} + R_{S2}R_{S3}}{R_{S2}\left(R_{S1} + R_{S3}\right)} V_{GQ2} \tag{7}$$

where V_{HS} is the upper hysteresis boundary and V_{LS} is the lower hysteresis boundary; V_{GQ2} is the gate threshold voltage of Q_{S2}; R_{S1}, R_{S2}, and R_{S3} are as shown in Fig. 6.

The load-sleep/load-on mode switching (e.g. t_1, t_2 and t_3 moments in Fig. 3) are controlled by the main MCU through software.

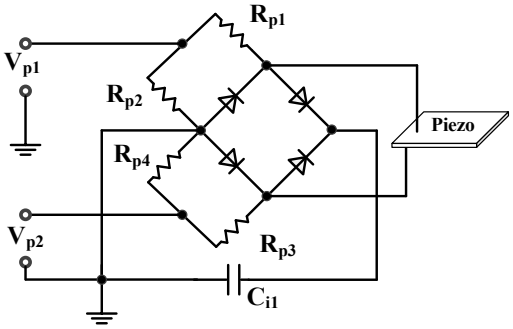

Fig. 7. Vibration measurement circuit

The piezo is used to provide energy and measure vibration. Fig. 7 shows the vibration measurement circuit. The bridge rectifier, C_{i1} and Piezo are the same devices shown in Fig. 2. R_{p1} and R_{p2} are the voltage divider for the positive voltage measurement. R_{p3} and R_{p4} are the voltage divider for the negative voltage measurement. In load-on mode, the main MCU records V_{p1} and V_{p2}, which contain the vibration information, and sends data to wireless system.

V. Experimental Results

A prototype (Fig. 8) has been built to verify the design. The components are listed in Table I.

TABLE I. COMPONENTS

Component	Value	Component	Value
R_1	5M ohm	C_1	330p F
R_2	5M ohm	U_1, U_2	TLV3691
R_{2-1}	2.5M ohm	Q_{h1}	IRML2244TR
R_3	5M ohm	Q_{c1}, Q_{c2}, Q_{h2}, Q_{S2}	BSS138N
R_4	5M ohm	R_{h1}	17M ohm
R_{4-1}	10M ohm	R_{h2}	5M ohm
R_5	5M ohm	R_{h3}	17M ohm
R_6	10M ohm	R_{h4}	10M ohm
R_7	1M ohm	R_{h1}	7.5M ohm
Boost Converter	BQ25504	R_{h2}	5M ohm
R_{h3}	1M ohm	R_{h4}	5M ohm

The threshold voltage of BSS138N is 0.6V. Based on (2) and (3), the hysteresis band of the buffers are 1.62V/2.64V. Based on (6) and (7), the load switch hysteresis band is 0.71V/1.5V. Note that the hysteresis band may be different from the calculated values because the threshold voltage varies.

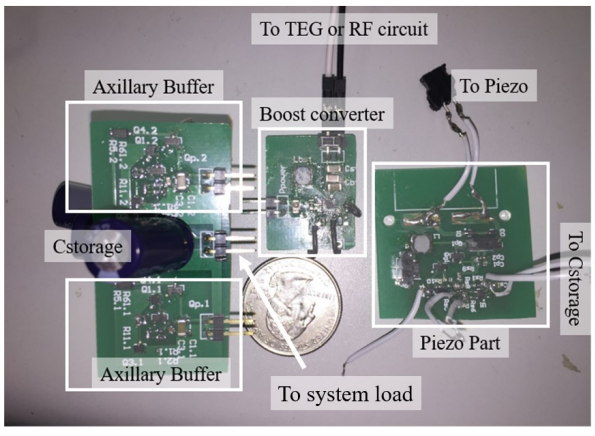

Fig. 8. Prototype

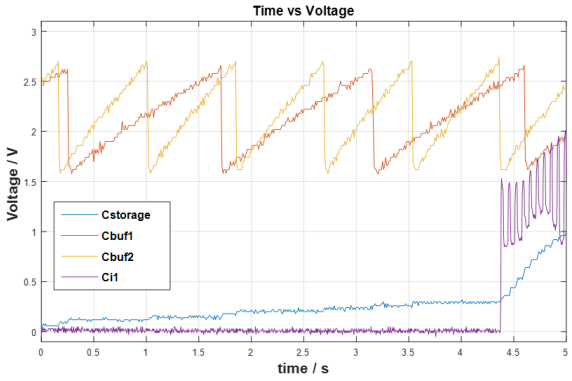

Fig. 9. Charging process. Blue –voltage of storage capacitor; red – voltage of buffer capacitor 1; orange – voltage of buffer capacitor 2; purple – voltage of piezo input capacitor C_{i1}

Based on (5), assuming $U_{in(max)}$ is 2.5V and $U_{buf(max)}$ is 3.4V, the maximum control power consumption is 6.08 µW. Comparing to MCU involved energy harvesting circuits, the control power consumption is significantly lower (for example: the power consumption of MSP432 ultra-low power MCU is 1.416 mW at 3V supply voltage and 4MHz CPU frequency).

The load-on mode duration time (T_{on}) is described in (8).

$$T_{on} = \frac{1}{2}\frac{C_{storage}\Delta V^2}{P_{load} - P_{eh}} \tag{8}$$

where ΔV is the voltage difference between load-on threshold and load-sleep threshold, P_{load} is the power consumption of load, P_{eh} is the energy harvesting power. For minimum T_{on} estimation, P_{eh} is neglected. The power consumption of MSP432, CC2650, temperature sensor (TMP103), and DC-DC converter (TPS60312) is 32mW. By using SCCR16B205SRB 2F capacitor, $T_{on}(\min) = \frac{1}{2} \times 2(1.5 - 0.71)^2 / 0.032 = 19s$.

A. Charging test

Fig. 9 shows a charging test. In this test, a 300 µF Capacitor is used as the storage unit instead of using 2F capacitor so that the charging process can be seen in a short time. The axillary source is a TEG. As shown in Fig. 9, during 0 to 4.4 seconds, the TEG module 1 (red) and the TEG module 2 (orange) are charging the storage capacitor. Their hysteresis band is 1.62 V and 2.64 V. Starting at 4.4 seconds, vibration happens at piezo port and piezo starts to charge the storage capacitor.

B. Load-on/load-off switching test

As described in section IV, these is hardware controlled load-on mode and load-off mode switching. In the load-on/load-off mode switching test, 2F ultra-cap is used as storage capacitor. Since this test focuses on discharging process, $C_{Storage}$ is charged with an external power source to shorten experiment time. As shown in Fig. 10, when time = 10s, the storage unit voltage increases to 1.5V, S_1 shown in Fig. 1 turns on and the

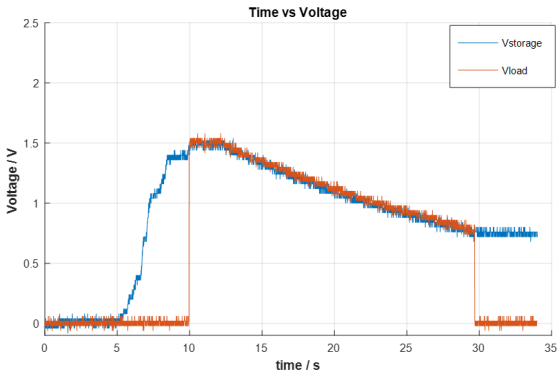

Fig. 10. Load-on and load-off switching test. Blue – voltage of storage capacitor; red – load voltage

load input voltage equals to the storage unit voltage. When time = 29s, the storage unit voltage decreases to 0.8V, S_1 turns off and the load input voltage is 0.

VI. Conclusion

In this paper, a power management system with an embedded harvesting-sensing multiplexing technology for the self-powered vibration and temperature wireless sensor used in motor condition monitoring applications has been proposed. The multi-source energy harvester minimizes the environment dependence. The all analog structure significantly decreases the power consumption of the control circuit. With the load-mode control strategy, the minimum sensing duration time is 19 seconds. Experiments are processed to test the basic functions.

References

[1] A. Emadi, "Transportation 2.0," *IEEE Power and Energy Magazine,* vol. 9, pp. 18-29, 2011.

[2] S. Nandi, H. A. Toliyat, and X. Li, "Condition monitoring and fault diagnosis of electrical motors-a review," *IEEE Transactions on Energy Conversion,* vol. 20, pp. 719-729, 2005.

[3] Y. Da, X. Shi, and M. Krishnamurthy, "Health monitoring, fault diagnosis and failure prognosis techniques for Brushless Permanent Magnet Machines," in *2011 IEEE Vehicle Power and Propulsion Conference*, 2011, pp. 1-7.

[4] B. M. Ebrahimi and J. Faiz, "Magnetic field and vibration monitoring in permanent magnet synchronous motors under eccentricity fault," *IET Electric Power Applications,* vol. 6, pp. 35-45, 2012.

[5] S. S. Goundar, M. R. Pillai, K. A. Mamun, F. R. Islam, and R. Deo, "Real time condition monitoring system for industrial motors," in *2015 2nd Asia-Pacific World Congress on Computer Science and Engineering (APWC on CSE)*, 2015, pp. 1-9.

[6] Z. Wang, F. Bouwens, R. Vullers, F. Petré, and S. Devos, "Energy-autonomous wireless vibration sensor for condition-based maintenance of machinery," in *2011 IEEE SENSORS Proceedings*, 2011, pp. 790-793.

[7] J. Moon, P. Lindahl, J. Donnal, S. Leeb, L. R. Zachar, L. W. Cotta, *et al.*, "A nonintrusive magnetically self-powered vibration sensor for automated condition monitoring of electromechanical machines," in *2016 IEEE AUTOTESTCON*, 2016, pp. 1-7.

[8] J. Colomer-Farrarons, P. Miribel-Catala, A. Saiz-Vela, and J. Samitier, "A Multiharvested Self-Powered System in a Low-Voltage Low-Power Technology," *IEEE Transactions on Industrial Electronics,* vol. 58, pp. 4250-4263, 2011.

[9] E. Sardini and M. Serpelloni, "Self-Powered Wireless Sensor for Air Temperature and Velocity Measurements With Energy Harvesting Capability," *IEEE Transactions on Instrumentation and Measurement,* vol. 60, pp. 1838-1844, 2011.

[10] S. Bandyopadhyay and A. P. Chandrakasan, "Platform Architecture for Solar, Thermal, and Vibration Energy Combining With MPPT and Single Inductor," *IEEE Journal of Solid-State Circuits,* vol. 47, pp. 2199-2215, 2012.

[11] D. Carli, D. Brunelli, L. Benini, and M. Ruggeri, "An effective multi-source energy harvester for low power applications," in *2011 Design, Automation & Test in Europe*, 2011, pp. 1-6.

[12] C. C. Chen, T. K. Chung, C. Y. Tseng, C. F. Hung, P. C. Yeh, and C. C. Cheng, "A Miniature Magnetic-Piezoelectric Thermal Energy Harvester," *IEEE Transactions on Magnetics,* vol. 51, pp. 1-9, 2015.

[13] Y. Sang, X. Huang, H. Liu, and P. Jin, "A Vibration-Based Hybrid Energy Harvester for Wireless Sensor Systems," *IEEE Transactions on Magnetics,* vol. 48, pp. 4495-4498, 2012.

[14] H. Lhermet, C. Condemine, M. Plissonnier, R. Salot, P. Audebert, and M. Rosset, "Efficient Power Management Circuit: From Thermal Energy Harvesting to Above-IC Microbattery Energy Storage," *IEEE Journal of Solid-State Circuits,* vol. 43, pp. 246-255, 2008.

[15] A. Romani, M. Filippi, and M. Tartagni, "Micropower Design of a Fully Autonomous Energy Harvesting Circuit for Arrays of Piezoelectric Transducers," *IEEE Transactions on Power Electronics,* vol. 29, pp. 729-739, 2014.

[16] C. Shi, B. Miller, K. Mayaram, and T. Fiez, "A Multiple-Input Boost Converter for Low-Power Energy Harvesting," *IEEE Transactions on Circuits and Systems II: Express Briefs,* vol. 58, pp. 827-831, 2011.